Digest Journal of Nanomaterials and Biostructures Vol. 16, No. 4, October-December 2021, p. 1619-1625

Nanostructure of carbonated hydroxyapatite precipitation extracted from pearl shells (Pinctada maxima) by pH treatment

R. Anggraini[a], M. Sari[a], Aminatun[b], T. Suciati[c], K. Dahlan[d], Y.Yusuf[a,*]
[a]*Department of Physics, Universitas Gadjah Mada, Yogyakarta 55281, Indonesia*
[b]*Department of Physics, Universitas Airlangga, Surabaya 60115, Indonesia*
[c]*Department of Pharmaceutics, Institut Teknologi Bandung, Bandung 40116, Indonesia*
[d]*Department of Physics, Institut Pertanian Bogor, Bogor 16680, Indonesia*

Carbonated hydroxyapatite (CHA) was successfully synthesized from pearl shells (*Pinctada maxima*) using the precipitation method with pH treatment variation. Based on the X-ray diffractometer (XRD) results, pH treatment caused the crystallographic properties of CHA to decrease. The Fourier transform infrared spectroscopy (FTIR) data showed the characteristics of B-type CHA. The energy dispersive X-Ray spectroscopy (EDS) analysis showed that CHA synthesized with a pH of 10 had the most significant carbonate content of 6.3 wt%. Based on the transmission electron microscopy (TEM) analysis, the morphology of CHA with a pH of 10 was the most agglomerated compared to the other samples.

(Received July 10, 2021; Accepted December 13, 2021)

Keywords: Carbonated hydroxyapatite, Nanostructure, Pearl shells, pH effect, Bone tissue engineering application

1. Introduction

Hydroxyapatite (HA; $Ca_{10}(PO_4)_6(OH)_2$), which is from the calcium phosphate family [1, 2], are alternative materials used in orthopedic, dental, and maxillofacial applications [3]. HA has the lattice parameters of a = 9.433Å and c = 6.875Å, and a variable Ca/P molar ratio of 1.67 [4-7]. The advantages of HA are its bioactivity, biocompatibility, and non-corrosiveness [4,8]. HA is also the most stable phase of Ca/P crystals. HA's weight is 69% of that of pure bone, and it is the most stable compound in body fluids and dry air up to a temperature of 1200℃ [9]. Since most of the mineral fraction in human bone tissue has the HA structure, and it can effectively reconstruct human bone tissue [10].

The natural bone composition contains the ion carbonate $(CO_3)^{2-}$ which varies based on age. Depending on age, bones have 2–8 wt% carbonate [11-15] in their total weight, which differs from other bone-forming elements, such as Na^{2+}, Mg^{2+}, K^+, F^-, and Cl^-. Due to carbonate minerals in natural bones, substituting HA with carbonate minerals is called carbonated hydroxyapatite (CHA) [11-17]. The particle size of CHA is known to be smaller than the particle size of HA, so tissue interaction with CHA will be better [18]. As a result, CHA has been developed as a bioceramic alternative for bone tissue engineering applications [13].

CHA ($Ca_{10-x}(PO_4)_{6-x}(CO_3)_x(OH)_{2-x}$ with $0 \le x \le 2$) can be divided into three types [17]: B-type (the carbonate ion replaces the phosphate ion), A-type (the carbonate ion replaces the hydroxyl ion), and AB-type (the carbonate ion replaces the phosphate and hydroxyl ions simultaneously). In bone tissue engineering applications, B-type CHA is the most widely used [11-20]. Generally, B-type CHA can reabsorb osteoclasts and is highly soluble in apatite lattices in both in-vitro assays [13]. In B-type CHA, the combination of carbonate ions and tetrahedral phosphates causes the alteration in lattice parameters of the hexagonal structure of CHA [19]. B-type CHA can decrease a value lattice parameter and increase c value lattice parameter c.

Synthetic CHA can be obtained through the reaction of synthetic compounds and the reaction of natural compounds. Natural compounds, such as biogenic materials must contain

* Corresponding author: yusril@ugm.ac.id

calcium. Biogenic materials are derived from materials, such as some shells and bones [20]. In this work, pearl shells (*Pinctada maxima*) from Indonesia were used as the natural compound for chemical synthesis [11,17,22]. The Central Bureau of Statistics of marine and coastal resources noted that the cultivation of pearl shells in Indonesia is one type of shellfish cultivation that was developing because it has excellent potential as a source of calcium carbonate, easy to produce, and inexpensive [11,17].

A variety of CHA synthesis techniques have been developed, including co-precipitation [11-17,19-20], nano emulsion [23,24], sol-gel [25,26], mechanical alloying [27], and mechanochemical-hydrothermal methods [28,29]. In this work, the co-precipitation method was selected to synthesize CHA because this method can produce nano-sized apatite particles. The temperature synthesis and pH treatment can control the precipitated particle sizes [30]. Moreover, this is a simple process with large output for large-scale (i.e., industrial) production. Significantly, the physical and chemical structure of the nanostructure can influence the character of cell in contact with the surface [31,32]. Therefore, to determine whether the sample synthesized was nanometer size, and it was necessary to characterize using TEM (Transmission Electron Microscopy). TEM analysis also can be used to analyze the morphology and particle size distribution of the CHA.

This work explores the potency of pearl shells (*Pinctada maxima*) from Indonesia as the source of calcium in CHA synthesis. In previous research [11], CHA with pH variations at 8,9, and 10 have been fabricated with the stirring time of CHA solutions at 30 min and the nanostructure using TEM analysis is not explored. In this work, CHA is synthesized using the precipitation method with a stirring time of 4 h and pH variations treatment at 8, 9, and 10. The physicochemical characteristics of this CHA are observed, including its effect on nanostructure, crystallographic properties, the molar ratio of Ca/P, and its functional groups.

2. Experimental

2.1. Materials

The pearl shells used as a biogenic material were taken from Bali, Indonesia. The precursors of diammonium hydrogen phosphate ($(NH4)_2 HPO_4$), sodium bicarbonate ($NaHCO_3$), and ammonium hydroxide (NH4OH) solution were purchased from Merck (USA).

2.2. Preparation of Calcium Oxide (CaO)

The CaO was fabricated in previous research [11,17], so this work used these samples.

2.3. Synthesis of CHA

Based on previous research [17], an amount of 0.06 mol of CaO powder was mixed with 80 mL of distilled water for 1 h with a stirring velocity of 300 rpm at room temperature until solution formed calcium hydroxide ($Ca(OH)_2$. Then, 0.036 mol of $(NH_4)_2HPO_4$ was mixed with 80 ml of distilled water for 1 h with a stirring velocity of 300 rpm at room temperature. The pH was controlled by adding 10−15 ml of NH_4OH at 25% into the $(NH_4)_2HPO_4$ solution while still stirring until a $(NH_4)_2HPO_4$ solution was formed in alkaline conditions. An amount of 0.036 mol of NH_4HCO_3 was mixed with 80 ml of distilled water for 1 h with a stirring velocity of 300 rpm at room temperature. Then, the NH_4HCO_3 solution was slowly added dropwise to the $(NH_4)_2HPO_4$ solution at a rate of 1 ml/min at room temperature while stirring until the carbonate-phosphate solution was formed. The carbonate-phosphate solution was slowly added dropwise at 40 ml/min to the $Ca(OH)_2$ solution. The liquid mixture was stirred at a velocity of 300 rpm for 30 min. In this work, the pH treatments of 8, 9, and 10 of the mixture were used by adding ammonium hydroxide (NH_4OH, 25%) 3M. The mixture was stirred at a velocity of 300 rpm for 4 h at a temperature of 60℃. The solution was subjected to an aging treatment for 24 h and was filtered using filter paper for 24 h to obtain the samples' precipitate. After the filtering process, the sample was put in an oven at a temperature of 100℃ for 24 h to remove the moisture content until a dry CHA

compound was formed. Finally, CHA was calcined at a temperature of 650℃ for 2 h using a furnace.

2.4. Characterization of CHA particles

2.4.1. Morphology, Particle Size Distribution and Aspect Ratio Analysis

The morphology of the CHA particle was observed by TEM (Joel Jem-1400, Japan). The particle size distribution, polydispersity, and aspect ratio of the CHA based on morphology data were calculated based on the measurements of 20 randomly selected particles using ImageJ software version 1997 (Laboratory for Optical and Computational Instrumentation, University of Wisconsin).

2.4.2. Composition of the CHA Powders

The EDS, included in the scanning electron microscopy (SEM, Joel JSM-6510LA-1400, Japan) tests were used to determine the carbon, calcium, and phosphorus composition of the CHA powders, and these results were used to calculate the molar ratio of Ca/P in the CHA powders.

2.4.3. Crystallography Analysis

The crystallographic properties of the CHA powders were determined by XRD (PAN analytical Type X'Pert Pro, Japan). The XRD data were recorded in the range $2\theta: 5 - 60°$ using $\mathrm{Cu} - \mathrm{K}\alpha$ radiation at $\lambda = 0.154$ nm [14].

2.4.4. FTIR Analysis

FTIR (Thermo Nicolet iS10, Japan) was conducted to analyze the functional groups of the CHA powders. Separately, the powder was ground and mixed with potassium bromide (KBr) and then passed into compact tablets [14].

3. Results and Discussion

3.1. XRD analysis

As shown in the XRD results (Fig. 1), the pattern formed was characteristic of B-type CHA with a stirring time of 4 h and a pH treatment of 8, 9, and 10 and matched with the Joint Committee on Powder Diffraction Standards **(**JCPDS) No. 19-0272. These formed three characteristic peaks at diffraction angles of 31.98°, 31.97°, and 31.92°, respectively. B-type CHA produced hexagonal crystalline shapes with an average lattice constant a = 9.4047 Å and c = 6.8960 Å [13]. Based on this result, CHA synthesized at pH 8, 9, and 10 approached the B-type CHA lattice constants (Table 1).

Table 1. Crystallographic properties of CHA synthesized with pH treatment variations.

Samples	Crystallite size (nm)	Microstrain	Crystallinity (%)	Lattice Parameter (Å)		
				a	*c*	*c/a*
CHA-pH 8	15.82 ± 2.46	0.0079	90	9.3695	6.8902	0.7353
CHA-pH 9	15.17 ± 1.64	0.0083	86	9.3695	6.8955	0.7359
CHA-pH 10	14.82 ± 1.77	0.0085	82	9.3695	6.8989	0.7363

The treatment of pH caused crystallographic properties of CHA to decrease. As shown in Table 1, the higher the pH treatment caused the lower the crystallinity level. Substitution of carbonate in HA inhibits crystal growth due to lattice defects in the apatite structure [17,20], thus reducing the crystallinity of the CHA powder and providing a smaller crystallite size, which is in agreement with the results obtained. The treatment of pH caused the microstrain to increase. The lower crystallinity also was indicated by the increasing microstrain in the CHA. The microstrain

was a form of crystal imperfection that appeared as a distortion or dislocation. A significant microstrain value showed a big amount of defect in the crystal [4]. Overall, the lower crystallinity was very good for bone growth because it caused dislocations so that cells could proliferate [14].

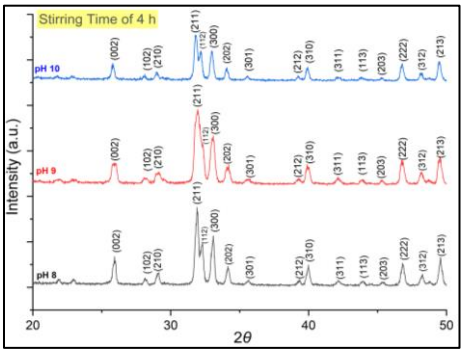

Fig. 1. XRD pattern of CHA synthesized with pH treatment variations.

3.2. FTIR analysis

FTIR spectroscopy was also used to determine the functional group of CHA. The synthesized CHA with pH treatments at 8, 9, and 10 exhibited the functional groups of B-type CO_3^{2-} at 876 cm^{-1} and 1460−1410 cm^{-1}, respectively. The FTIR test results (Fig. 2) show the characteristics of B-type CHA that were formed when the carbonate ions replaced the phosphate ions in the HA structure [12]. The PO_4^{3-} absorption was observed at 582−471 cm^{-1} and 1090−962 cm^{-1} for all pH treatments. The absorption of H_2O was observed at 3570 and 1640 cm^{-1}. Based on the FTIR data, there was a shift in the transmittance value of the carbonate and phosphate groups that tended to be lower and higher values along with the high pH treatments. In this result, CHA with the pH treatment of 10 could have a lower transmittance value, so the carbonate content of this CHA was indicated to be high. The higher carbonate content in CHA also caused the smaller crystallite size of this sample. This data also supports the XRD and EDS analysis.

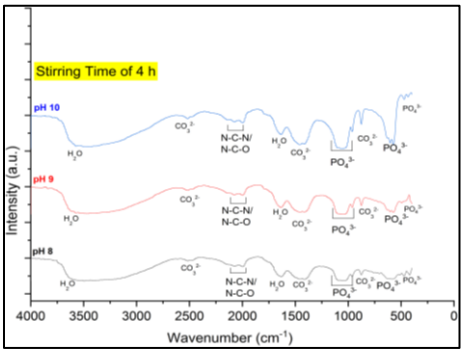

Fig. 2. FTIR spectra of CHA synthesized with pH treatment variations.

3.3. Composition of the CHA Powders

Based on data in Table 2, the extension of pH caused an increase in carbonate composition where the amount of carbonate was 2−6 wt%. As discussed in the introduction, bones were about 2−8 wt% of carbonate. CHA synthesized with a pH of 10 had the most significant carbonate content of 6.3 wt%. This data confirms that the treatment of pH caused carbonate content to increase [11,30,31]. Increasing the amount of carbonate affected the Ca/P molar ratio of the sample. The synthesized B-type CHA showed that the carbonate ion replaced the phosphate ion and that the increased carbonate caused the phosphate content to decrease. The FTIR spectra

support this result. Therefore, the Ca/P molar ratio will be even higher. The EDS analysis results show that the Ca/P mole ratio may increase when the pH increases.

Table 2. Element composition of CHA synthesized with pH treatment variations.

Samples	Carbonate content (wt%)	Ca/P molar ratio
CHA-pH 8	3.62 ± 0.40	1.97 ± 0.83
CHA-pH 9	5.25 ± 0.73	2.01 ± 0.13
CHA-pH 10	6.30 ± 0.85	2.27 ± 0.31

3.4. TEM analysis

The morphology of CHA with the pH variation can be seen in Fig. 3. As shown in Fig.1, the morphology of CHA with a pH of 10 was the most agglomerated compared to the other samples, and the shape of the sample grains was almost the same, namely an irregular circle [11,30,33]. This sample had large and uneven clumps and particle shapes, and the whole CHA looked irregular [34]. The pH values were significant in changing the sample's morphology [11].

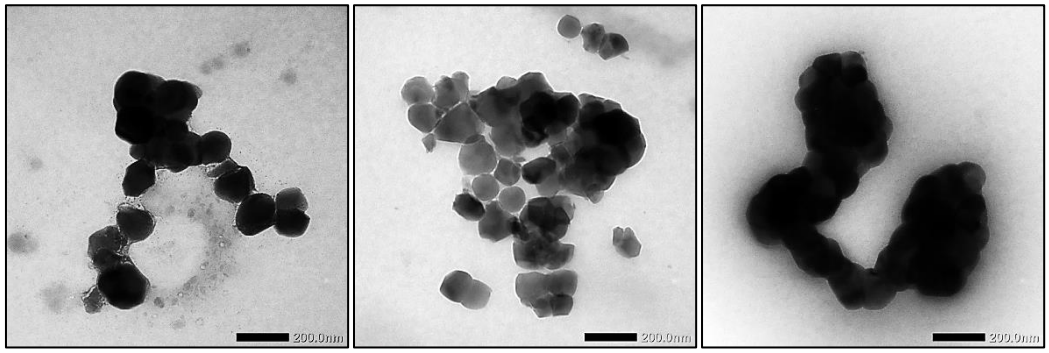

(a) *(b)* *(c)*

Fig. 3. Morphology of CHA with pH treatment variations: (a) pH 8, (b) pH 9, and (c) pH 10.

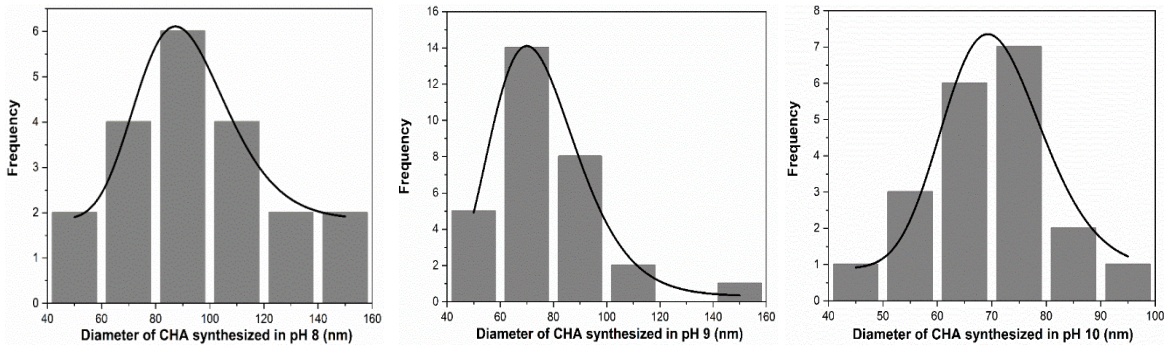

(a) *(b)* *(c)*

Fig. 4. Particle size distribution of CHA with pH treatment variations: (a) pH 8, (b) pH 9, and (c) pH 10.

The morphology results are supported by analyzing the particle size and polydispersity using ImageJ software, as shown in Table 3 and Fig. 4. Based on these data, the nanometer-sized B-type CHA particles were successfully obtained. From these data, the treatment of pH caused the particle size to decrease. All data pertaining to particle size shows a more normal distribution while the degree of aggregation increased [30,35]. This is supported by the polydispersity data where pH treatment caused the polydispersity to decrease, as shown in Table 3. The polydispersity was related to the diversity of the same sample size when analyzing the particle size distribution data. From data in Table 1 and Table 3, there was a strong mismatch factor between the crystallite size from XRD and TEM because the precipitation method depends on variables such as pH, stirring time, and so on. Some of parameters have not been controlled perfectly.

Table 3. Particle size distribution, polydispersity, and aspect ratio (length/width) analysis of CHA with pH variations.

Samples	Particle size (nm)	Polydispersity (%)	Aspect ratio
CHA-pH 8	90.44 ± 1.34	98.51	1.011
CHA-pH 9	73.69 ± 1.12	98.48	1.047
CHA-pH 10	70.43 ± 1.70	97.58	1.014

The length and width of 20 particles were measured to obtain an average value, and this was then computed to get the ratio of length to width (aspect ratio). As shown in Table 3, the aspect ratio increased due to the increased pH in CHA. These results suggested increasing the aspect ratio was caused by the higher substitution of carbonate into the phosphate site in the cell lattice (B-type CHA), as confirmed by XRD results [30,33].

4. Conclusion

The characteristics of the B-type CHA samples, including nanostructures, crystallographic properties, carbonate content, and chemical processes, were influenced by the varied pH treatments. CHA synthesized at pH 8, 9, and 10 approached the lattice constants of B-type CHA. All the pH treatments caused the crystallographic properties of B-type CHA to decrease. As shown in the FTIR data, CHA with the pH treatment of 10 could have a lower transmittance value, so the carbonate content of this CHA was indicated to be high. Thus, the samples had the highest carbonate content. Based on the TEM analysis, the nanometer size of the B-type CHA particles was successfully obtained.

Acknowledgements

The authors are immensely grateful to the Ministry of Education, Culture, Research, and Technology, Republic of Indonesia for its Riset Kolaborasi Indonesia (RKI) Program 2020. The authors acknowledge the use of the facilities and the technical assistance of the Material Physics and Electronics Laboratory and the staff of the Integrated Laboratory for Research and Testing at Universitas Gadjah Mada, Indonesia. Additionally, the authors would like to thank Apri I. Supii for his support of the sample procurement.

References

[1] I. D. Ana, G. A. P Satria, A. H Dewi, R. Ardhani, Bioceramics for clinical application in regenerative dentistry, Springer Nature Singapore Pte Ltd,Singapore, 309 (2018).
[2] I. D. Ana, Bone substituting materials in dental implantology, Springer Nature Switzerland AG, Switzerland, 121 (2019).
[3] F. Y. Syafaat, Y. Yusuf Y, J. Nanoelectron. Mater **11**, 51 (2018).
[4] M. Sari, Y. Yusuf, J. Nanoelectron. Mater **11**(3), 357 (2018).
[5] M. Sari, Y. Yusuf, IOP. Conf. Ser: Mater. Sci. Eng **432**, 1 (2018).
[6] F. Y. Syafaat, Y. Yusuf, J. Nanoelectron. Mater **12**(3), 357 (2019).
[7] M.Sari, P. Hening, Chotimah, I.D.Ana, Y. Yusuf, Biomater.Res **25**, 2 (2021).
[8] N.C. Hashim, D. Nordin, Dig. J. Nanomater. Bios. **14** (2), 991 (2019).
[9] M. Saleha, N. Halik, Annisa, Sudirman, Subaer, Prosiding Pertemuan Ilmiah XXIX HFI **3**, 124 (2015).
[10] V.Mawuntu, Y. Yusuf, J. Asian. Ceram. Soc **7**(2), 1 (2019).
[11] R. M. Anggraini, A. I. Supii, G. B. Suparta, Y. Yusuf, Key Engineering Materials **818**, 44 (2019).
[12] H. A. Permatasari, A. I.Supii, G. B. Suparta, Y. Yusuf, Key. Eng. Mater **818**, 31 (2019).
[13] H. A. Permatasari, Y. Yusuf, IOP. Conf. Ser: Mater. Sci. Eng **546**, 042031 (2019).
[14] M.Sari, P. Hening, Chotimah, I.D.Ana, Y. Yusuf, Mater. Today. Comm **26**, 102135 (2021).
[15] M. Sari, P. Hening, N.A. Kristianto, Chotimah, I.D.Ana, Y. Yusuf, Coatings **11**, 941 (2021).
[16] M. Sari, P. Hening, N.A. Kristianto, Chotimah, I.D.Ana, Y. Yusuf, Coatings **11**, 1189 (2021).
[17] R. M Anggraini, Y. Yusuf, IOP. Conf. Ser: Mater. Sci. Eng, Malang **546**, 042002 (2019).
[18] M. Safarzadeh, S. Ramesh, C. Y. Tan, H. Chandran, A. Fauzi, M. Noor, S. Krishnasamy, U. J. Alengaram, S. Ramesh, Ceram. Int. **45** (3), 3473 (2019).
[19] Almukarrama, Y. Yusuf, IOP.Conf. Ser: Mater. Sci. Eng **546**, 042001 (2019).
[20] R. Wati, Y. Yusuf, Key. Eng. Mater **818**, 37 (2019.
[21] Y. Rizkayanti, Y. Yusuf, J. Nanoelectron. Mater **12**(1), 85 (2019).
[22] N. Vujasinović-stupar, S. Novković, I. Jezdić, Serbian Arch. Med. **137**, 518 (2009).
[23] W. Y. Zhou, M. Wang, W. L. Cheung, B. C. Guo, D. M. Jia, J. Mater. Sci: Mater. Med. **19**, 103 (2008).
[24] I. Ezekiel, S. R. Kasim, Y. M. B. Ismail, A. M. Noor, Ceram. Int **44**(11), 13082 (2018).
[25] M. H. Fathi, A. Hanifi, V. Mortazavi, J. Mater. Proceed. Tech **2**(1-3), 536 (2007).
[26] A. Behnamghader, A. Kazemzadeh, Mater. Sci. Eng C **28**(8), 1326 (2008).
[27] S. Lala, S. Brahmachari, P. K. Das, D. Das, T. Kar, S. K. Pradhan, Mater.Sci. Eng C **42**, 647 (2014).
[28] T. S. S. Kumar, I. Manjubala, J. Gunasekaran, Biomater **21**(16), 1623 (2000).
[29] W. Kong, K. Zhao, C. Gao, P. Zhu, Mater. Lett **255**, 126552 (2019).
[30] R. Othman, Z. Mustafa, C. W. Loon, A. F. M. Noor, Procedia. Chem **19**, 539 (2016).
[31] E. M. Christenson, K. S. Anseth, J. J. J. P. V. D. Beucken, C. K. Chan, B. Ercan, J. A. Jansen, C. T. Laurencin, W. J. Li, R. Murugan, L. S. Nair, S. Ramakrishna, R. S. Tuan, T. J. Webster, A. G. Mikos, J. Ortho. Res **25**(1), 11 (2007).
[32] F. Abolaban, F. Djouider, Dig. J. Nanomater. Bios. **13** (3), 649 (2020).
[33] Y. Wu, Y. Lee, H. Chang, Mater. Sci. Eng. C **29**(1), 237 (2009).
[34] V. Jokanovic, D. Izvonar, M. D. Dramicanin, B. Jokanovic, V. Zivojinovic, D. Markovic, B. Dacic, J. Mater. Sci: Mater. Med **17**, 539 (2006).
[35] M. A. Goldberg, V. V. Smirnov, D. D. Titov, L. I. Shvorneva, E. A. Kudryavtsev, D. A. Kolesnikov, S. M. Barinov, Doklady. Chem **456**(79-82), 177 (2014).